Spectrally Matched Quantum Dot Photoluminescence in GaAs-Si Tandem Luminescent Solar Concentrators

David R. Needell, Colton R. Bukowsky, Sunita Darbe, Haley Bauser, Ognjen Ilic, and Harry A. Atwater

***Abstract*—Luminescent solar concentrators (LSCs) can capture both direct and diffuse irradiance via isotropic absorption of waveguide-embedded luminophores. Additionally, LSCs have the potential to reduce the overall cost of a photovoltaic (PV) module by concentrating incident irradiance onto an array of smaller cells. Historically, LSC efficiencies have suffered in part from incomplete light absorption and non-unity quantum yield (QY) of the luminophores. Inorganic quantum dot (QD) luminophores allow the spectral tuning of the absorption and photoluminescence bands, and have near-unity QYs. In a four-terminal tandem LSC module scheme, visible light is trapped within the LSC waveguide and is converted by GaAs cells, and near infrared light is optically coupled to a Si subcell. Here, we investigate the efficiency of a GaAs/Si tandem LSC as a function of luminophore absorption edge and emission wavelength for QD luminophores dispersed in an LSC waveguide with embedded, coplanar GaAs cells. We find that positioning the luminophore absorption edge at 660 nm yields a maximum module power efficiency of approximately 26%, compared with 21% for the non-optimized luminophore and 19% for the bare Si cases.**

***Index Terms*—III-V and concentrator photovoltaic (PV), luminescent devices, Monte Carlo methods, quantum dots (QDs), tandem PV.**

I. Introduction

OVER the past few decades, there has been an increased interest in luminescent solar concentrators (LSCs) as a low-cost alternative to traditional geometric concentrators and single-junction photovoltaic (PV) modules. LSCs, commonly referred to as active concentrators, absorb incident sunlight isotropically via luminophores embedded in a planar waveguide. The luminophores then radiate light at longer wavelengths into the planar waveguide, and the emitted light propagates within the waveguide, trapped via total internal reflection. This trapped photoluminescence (PL) can then be concentrated onto solar cells, which are arranged to either lie perpendicular to the plane at the waveguide edge [see Fig. 1(a)] or in a coplanar orientation parallel to the waveguide [see Fig. 1(b)] [1]–[3].

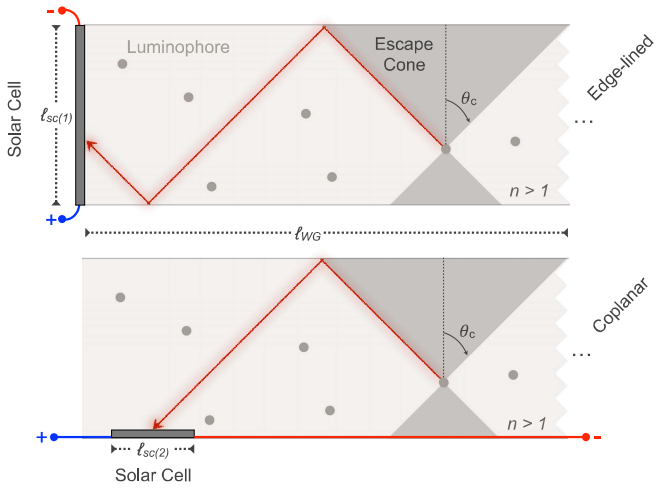

Fig. 1. Two-dimensional schematic of an LSC in the (top) edge lining and (bottom) coplanar orientations of the solar cell. Here, θc is the critical angle of the escape cone.

Despite growing interest in using LSCs for diffuse light sunlight concentrator PVs [4], overall power conversion efficiencies (PCEs) of LSCs remain limited [5], [6]. Most notably, the luminophore absorption only covers a portion of the incident solar spectrum. Further, nonradiative recombination by the luminophores and incomplete light trapping by the waveguide can significantly decrease the number of photons incident on the solar cell [7]. With such limited efficiencies, LSC applications have traditionally focused on multifunctional uses, such as building integrated PVs [8].

In order to achieve higher PCEs, previous reports have explored various organic and inorganic luminophores and their effect on LSC module optical efficiency (OE) [5]. While numerous photoconverter species have been employed in LSCs, many exhibit limited PL quantum yield (PLQY). To address this, previous works explored the use of inorganic quantum dot (QD) luminophores in active concentrators [8]–[17]. Core/shell QDs have been demonstrated to exhibit large Stokes shifts and

Manuscript received September 18, 2018; revised December 1, 2018; accepted December 20, 2018. Date of publication January 22, 2019; date of current version February 18, 2019. This work was supported in part by the Advanced Research Projects Agency under Energy (ARPA-E) under Award DE-AR0000627 and in part by the Office of Energy Efficiency and Renewable Energy (EERE) under Award EEC-1041895. *(Corresponding author: Harry A. Atwater.)*

D. R. Needell, C. R. Bukowsky, H. Bauser, O. Ilic, and H. A. Atwater are with the Department of Applied Physics, California Institute of Technology, Pasadena, CA 91125 USA (e-mail: dneedell@caltech.edu; cb@caltech.edu; hbauser@caltech.edu; ilic@caltech.edu; haa@caltech.edu).

S. Darbe is with the Materials Science Department, Spiber Inc., Yamagata 997-0052, Japan (e-mail: sunitadarbe@gmail.com).

This paper has supplementary downloadable material available at http://ieeexplore.ieee.org, provided by the authors.

Digital Object Identifier 10.1109/JPHOTOV.2019.2892075

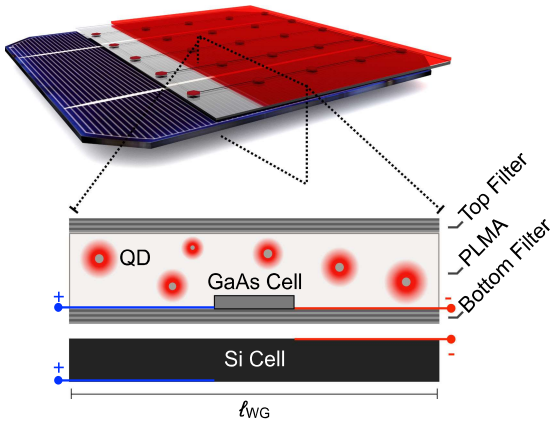

Fig. 2. Conceptual rendering of the tandem LSC/Si module (top) and its cross section (bottom). The cross section shows a single unit cell of the full tandem device architecture, and indicates electrical connections to the top and the bottom cell.

maintain near-unity PLQY, where the choice of materials and QD size can blue or red shift the absorption band edge and PL emission peak [18].

We have shown in previous work that tandem-on-Si LSC designs could allow for efficiencies beyond the Shockley–Queisser limit for single junction Si PV devices [19]. However, the QDs used in that design did not have optimal spectral absorption and emission characteristics to enable the highest overall module efficiency. Here, we treat the luminophore absorption and emission wavelengths as variable parameters, and explore the achievable efficiency limits that could be obtained by redshifting the luminophore absorption and PL in an LSC optically coupled to a flat-plate Si cell. This four-terminal (4T) tandem employs a coplanar GaAs LSC top-cell configuration and a standard, commercially available passivated emitter rear contact (PERC) Si subcell. Fig. 2 shows the schematic of the tandem LSC/Si device. Using a Monte Carlo ray tracing modeling tool, we simulate the overall module performance of such a tandem LSC/Si device and explore the implications of further redshifting the luminophore spectral features for a variety of PLQYs and QD concentration within the polymeric waveguide.

II. Tandem LSC Modeling

A. Monte Carlo Ray Tracing

As seen in Fig. 2, we configure an LSC top cell in tandem with a Si subcell to use as a 4T device. By relying upon short wavelength absorption in the embedded luminophores, re-radiated light trapped within the polymer waveguide impinges upon the higher bandgap GaAs embedded cell. Longer wavelength light beyond the GaAs band edge propagates with low loss in the LSC layer, and transmits through to reach the underlying PERC Si cell.

For this coplanar LSC configuration, the geometric gain (GG) can be determined by comparing the cell area, with length $l_{\mathrm{sc}(2)}$, and the waveguide aperture area l_{WG} as shown in Fig. 1. This geometry allows a given GG to be maintained for arbitrarily large module areas, thus enabling the coplanar configuration to have higher LSC photocurrents relative to an edge-lining cell configuration [9], [19].

We simulate the IV performance of this 4T LSC/Si module using a Monte Carlo ray tracing algorithm [19]. The stochastic model traces incident photons through the layers, which are initialized to strike the top filter of the tandem stack. We calculate contributions to photon propagation from scattering, reflection, transmission, and absorption characteristics for each as functions of photon wavelength and angle of incidence. We initialize approximately 10^6 photons for a given simulation across a wavelength range from 300 to 1100 nm, where we scale incident photon power by the AM1.5 g spectrum.

To determine the luminophore absorption and PL excitation rate, we apply the Beer–Lambert law, given a specific QD concentration within the poly(lauryl methacrylate) (PLMA) waveguide layer whose average index of refraction is 1.44 across the visible spectrum. We generate PL profiles according to the probability distribution of the photoconverter species, where the PLQY determines the probability for radiative recombination. Further information on the algorithm and the implementation can be found in the supporting information (SI) for this paper.

Short-circuit current density (*J*sc) is modeled by the Monte Carlo ray tracing algorithm, taking into account the GaAs/Si cell reflectance and internal quantum efficiency. We apply a detailed balance model to calculate open-circuit voltage (*V*oc) and fill factor (FF) for the GaAs and PERC Si cells. We include radiative and nonradiative dark current density contributions for each cell type, given by

$$V_{\mathrm{oc}} = \frac{nk_BT}{q}\ln\left(\frac{I_L}{I_0}\right) + \frac{nk_BT}{q}\ln(Q_{\mathrm{ERE}})$$

where q is the electron charge, k_{B} is the Boltzmann constant, T is the cell operating temperature where we assume room temperature, I_{L} is the simulated photocurrent under AM1.5 g spectrum, I_0 the dark current in the radiative limit, and Q_{ERE} is the external radiative efficiency [20], [21]. We model Q_{ERE} following literature procedures related to the external quantum efficiency (EQE) of each cell. We assume a GaAs microcell of dimensions 400 by 400 μm and assume a GG of 50, yielding a waveguide unit cell area of 8 mm. We apply periodic boundary conditions to simulate a larger array.

B. Model Validation

We validate this Monte Carlo ray trace and detailed balance model with experimental performance matching and literature comparison. As a base case, we simulate a bare, zero-density QD waveguide onto such a PERC Si subcell and match to 1-sun, AM1.5 illumination of a measured PERC cell [22]. As a secondary base case, we compare the ray trace to measured GaAs III-V cells under 1-sun, AM1.5 illumination [23]. Table S1 of the SI details the simulation results' agreement with experimental measurements.

We also apply this ray-trace model to LSC studies, each employing a filter/QD waveguide architecture with a trench reflector for photon recapture [9], [19]. We find excellent agreement for varying QD concentration within the waveguide with

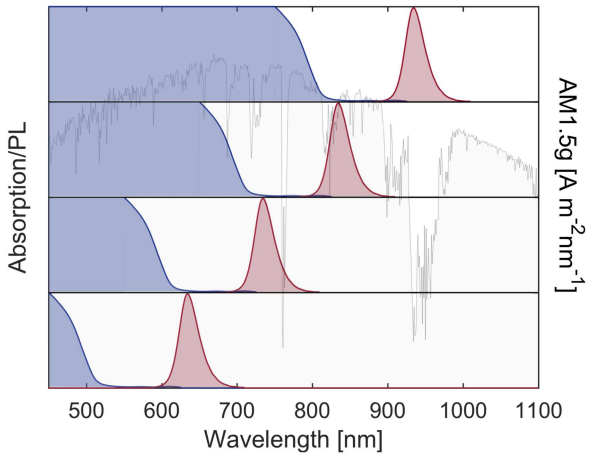

Fig. 3. Absorption (shaded blue) and PL (shaded red) spectra for varying red-shifted QD luminophores, employing the same absorption and PL band edge structure. The right axis corresponds to the AM1.5G spectrum.

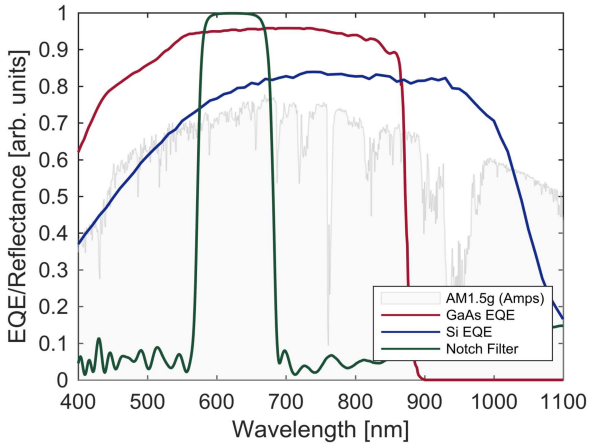

Fig. 4. EQE of the embedded GaAs and underlying IBC Si cells, referenced to the AM1.5G spectrum.

respect to harvested photocurrent. We include literature base case studies and Monte Carlo ray trace comparison in the SI for this paper and show excellent quantitative agreement between this Monte Carlo ray trace and prior work, as shown in Fig. S7 of the SI.

C. *Spectrally Matched Luminophores*

Inorganic QD luminophores span a wide wavelength range of absorption and PL features [18]. For instance, CdSe/CdS core/shell QDs typically exhibit absorption bands near 500 nm in wavelength, and PL peaks centered near 650 nm, whereas Cd1-xCuxSe QDs absorb further into the red, around 700 nm, and emit around 900 nm [17]. Here, we model the effects of spectrally-shifted absorption and PL bands on the overall module efficiencies of the tandem LSC/Si device. Fig. 3 shows the absorption and PL spectra for varying spectrally-shifted luminophores, assuming a constant PL distribution and absorption feature, for the sake of direct comparison.

We simulate applying top and bottom notch filters in this waveguide geometry as shown schematically in Fig. 2 and spectrally in Fig. 4. Previous studies show increased OE of the LSC component with the incorporation of such PL-concentrating mechanisms [1], [5], [9], [24], [25]. Such a notch filter features a high reflectance stopband centered around the luminophore PL regime and passbands in order to allow for maximum QD absorption (short wavelength) and PERC Si absorption (long wavelength). We make no assumption about the material or notch-filter design. However, we assume that the stopband of the filter remains centered around the PL peak for all angles of incidence. Such light-trapping filters traditionally derive from alternating high/low refractive index material in the form of a one-dimensional photonic crystal [26]–[28]; however, other designs, such as high contrast grating metasurfaces, also show promise as tunable notch filter designs [29]–[32].

Fig. 4 gives the EQE for both the embedded GaAs and underlying Si cells, plotted against the AM1.5 g spectrum as well as the simulated notch-filter reflectance.

III. Simulation Results

We investigate how the module efficiency of such an LSC/Si tandem changes with varying luminophore absorption and PL wavelength index. We find a peak in module efficiency and GaAs *J*sc/*V*oc under 1-sun illumination for luminophores exhibiting increased absorption edges out to 650 nm and PL peaks centered around 835 nm. Fig. 5 shows both the tandem PCE as well as the breakdown of GaAs LSC and PERC Si bottom cell efficiencies for the given PLQY of 0.98. As seen, we obtain maximum module PCE when the GaAs LSC top cell produces more power output than the PERC Si bottom cell.

Fig. 6 shows the *J*sc and *V*oc for the GaAs LSC top cell and PERC Si bottom cell with respect to varying QD absorption/PL shifting. We note an approximate 2.5 factor increase in *J*sc of the GaAs microcell for an optimized spectral position 18.1 mA/cm^2 relative to the unshifted CdSe/CdS case 7.09 mA/cm^2. We attribute such photocurrent increase because of increased light absorption across the incident solar spectrum. For further PL trapping, specifically to minimize photon loss through the waveguide escape cone, we assume a notch-filter spectrum as shown in Fig. 4, centered for all luminophore species around the PL center. Fig. 6 additionally shows the *V*oc of each the GaAs-embedded cell and the PERC Si subcell in this tandem configuration with top and bottom notch filters. In addition to varying the spectral features of the inorganic luminophore, we vary the PLQY. We apply constant PLQY values of 0.50, 0.90, 0.95, 0.98, and 1.00 across the PL profile. Both Figs. 5 and 6 demonstrate the substantial impact of PLQY on LSC performance. For values of 0.50 or lower, we find that further red-shifted luminophore features result in degraded PCE as a result of increased nonradiative recombination of incident photons by the luminophore species.

We see increased concentration of photocurrent arriving and collected by the GaAs microcell array, as shown in Fig. 7. With greater absorption of sunlight by the photoconverter species, a greater portion of incident sunlight is collected and redirected to the embedded cell.

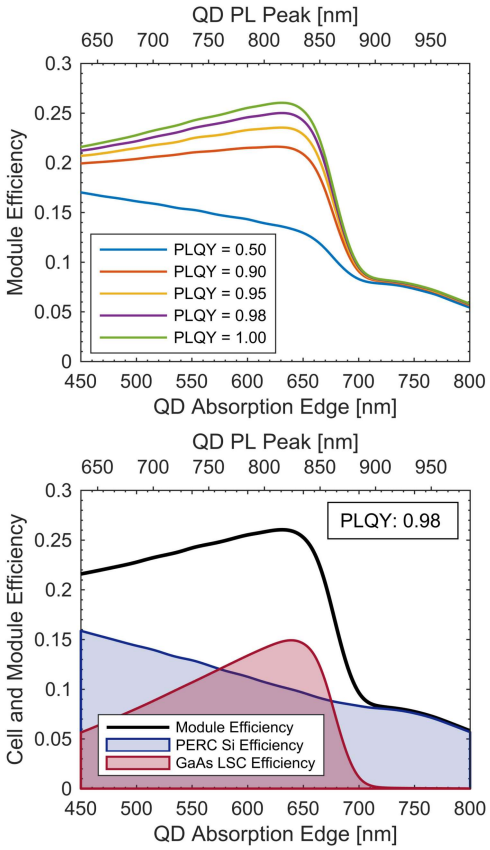

Fig. 5. Effects of luminophore redshifting on (top) the tandem LSC/Si module efficiency for varying PLQY and (bottom) the GaAs/Si individual cell efficiencies for the PLQY of 0.98.

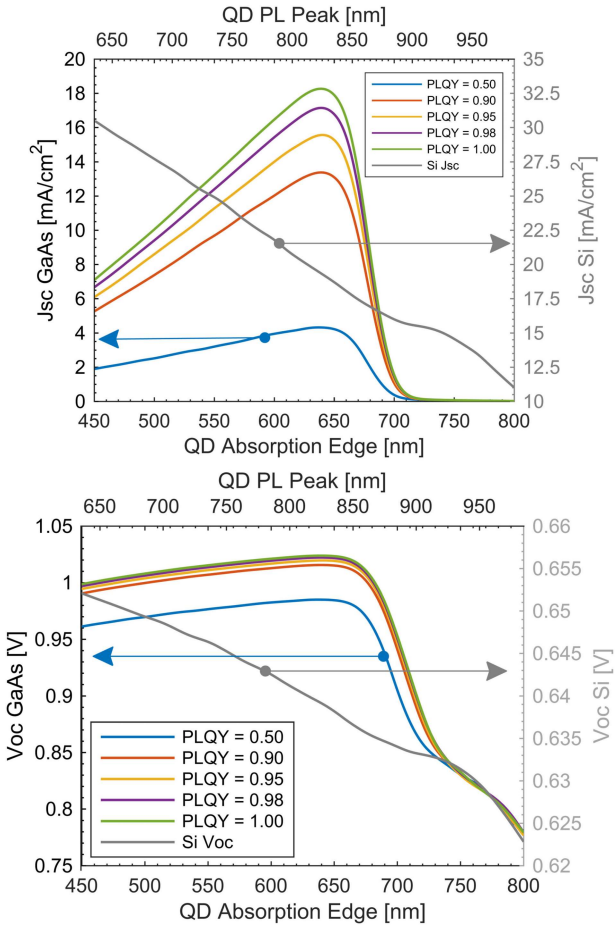

Fig. 6. Effects of luminophore redshifting on GaAs/Si (top) Jsc and (bottom) *V*oc.

IV. Summary and Conclusion

We have characterized the performance of a tandem LSC/Si module design where spectral position of the embedded luminophore absorption/emission is a design parameter. We rely on an experimentally validated Monte Carlo ray tracing modeling tool to estimate the overall power output for an LSC employing a PLMA waveguide with PL trapping, notch filters for increased photocurrent collection. To match increased absorption edge features of the luminophore, we couple PL to GaAs coplanar microcells in a dense array geometry of GG 50.

We find that for such an LSC design, there exists an ideal spectral position of the emission/absorption bands that maximizes module efficiency. Further, we show that for all PLQY values at or above 0.90, such a tandem device design benefits from increased redshifting of photoconverters. From this analysis, we conclude that tandem LSC devices exhibit strong PCEs for use as a potential high-performance PV candidate under a significant range of PLQY values.

Optimal performance characteristics result in a red-shifted luminophore with a PL profile centered around 835 nm and a Stokes shift of 100 nm. We find maximum PCE beyond 26% with both radiative and nonradiative contributions to the *V*oc and FF. We assume modeled PL-trapping notch filters encasing the spectrally shifted luminophores with a stopband width of approximately 100 nm at normal incidence, here. This result demonstrates the applicability of LSC/Si tandems with use of further red-shifted photoconverters in place of traditional III-V/Si tandem technologies.

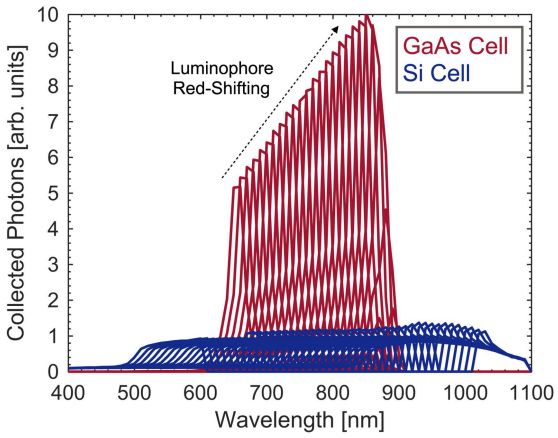

Fig. 7. Increase of collected photocurrent from the GaAs microcells of the tandem LSC/Si for continual redshifting of the QD luminophores up until the band edge.

REFERENCES

[1] U. Rau, U. W. Paetzold, and T. Kirchartz, "Thermodynamics of light management in photovoltaic devices," *Phys. Rev. B–Condens. Matter Mater. Phys.*, vol. 90, 2014, Art. no. 035211.

[2] G. C. Glaeser and U. Rau, "Collection and conversion properties of photovoltaic fluorescent collectors with photonic band stop filters," in *Proc. SPIE*, vol. 6197, 2006, pp. 61970L–61970L–11.

[3] J. Gutmann, H. Zappe, and J. C. Goldschmidt, "Predicting the performance of photonic luminescent solar concentrators," in *Proc. IEEE 39th Photovolt. Specialists Conf.*, 2013, pp. 1864–1868.

[4] M. G. Debije and V. A. Rajkumar, "Direct versus indirect illumination of a prototype luminescent solar concentrator," *Sol. Energy*, vol. 122, pp. 334–340, 2015.

[5] M. G. Debije and P. P. C. Verbunt, "Thirty years of luminescent solar concentrator research: Solar energy for the built environment," *Adv. Energy Mater.*, vol. 2, no. 1, pp. 12–35, 2012.

[6] W. G. J. H. M. Van Sark, Z. Krumer, C. D. M. Donegá, and R. E. I. Schropp, "Luminescent solar concentrators: The route to 10% efficiency," in *Proc. IEEE 40th Photovolt. Specialist Conf.*, 2014, pp. 2276–2279.

[7] C. Tummeltshammer, A. Taylor, A. J. Kenyon, and I. Papakonstantinou, "Losses in luminescent solar concentrators unveiled," *Sol. Energy Mater. Sol. Cells*, vol. 144, pp. 40–47, 2016.

[8] F. Meinardi *et al.*, "Highly efficient luminescent solar concentrators based on ultra-earth-abundant indirect band Gap silicon quantum dots," *Nat. Photon.*, vol. 11, no. 3, pp. 177–185, 2017.

[9] N. D. Bronstein *et al.*, "Quantum dot luminescent concentrator cavity exhibiting 30-fold concentration," *ACS Photon.*, vol. 2, pp. 1576–1583, 2015.

[10] A. J. Chatten, K. W. J. Barnham, B. F. Buxton, N. J. Ekins-Daukes, and M. A. Malik, "A new approach to modelling quantum dot concentrators," *Sol. Energy Mater. Sol. Cells*, vol. 75, no. 3–4, pp. 363–371, 2003.

[11] J. Madrid, M. Ropp, D. Galipeau, and S. May, "Investigation of the efficiency boost due to spectral concentration in a quantum-dot based luminescent concentrator," in *Proc. IEEE 4th World Conf. Photovolt. Energy Conf.*, 2006, pp. 154–157.

[12] F. Purcell-Milton and Y. K. Gun'ko, "Quantum dots for luminescent solar concentrators," *J. Mater. Chem.*, vol. 22, no. 33, pp. 16687–16697, 2012.

[13] I. Coropceanu and M. G. Bawendi, "Core/shell quantum dot based luminescent solar concentrators with reduced reabsorption and enhanced efficiency," *Nano Lett.*, vol. 14, no. 7, pp. 4097–4101, 2014.

[14] K. W. J. Barnham, J. Luis-Marques, J. Hassard, and P. O'Brien, "Quantum dot concentrator and a model for global red-shift," *Appl. Phys. Lett.*, vol. 76, no. 9, 2000, Art. no. 1197.

[15] F. Meinardi *et al.*, "Large-area luminescent solar concentrators based on /'Stokes-shift-engineered/' nanocrystals in a mass-polymerized PMMA matrix," *Nat. Photon.*, vol. 8, no. 5, pp. 392–399, 2014.

[16] N. D. Bronstein *et al.*, "Luminescent solar concentration with semiconductor nanorods and transfer-printed micro-silicon solar cells," *ACS Nano*, vol. 8, no. 1, pp. 44–53, 2014.

[17] L. R. Bradshaw, K. E. Knowles, S. McDowall, and D. R. Gamelin, "Nanocrystals for luminescent solar concentrators," *Nano Lett.*, vol. 15, no. 2, pp. 1315–1323, 2015.

[18] A. P. Alivisatos, "Semiconductor clusters, nanocrystals, and quantum dots," *Sci.*, vol. 271, pp. 933–937, 1996.

[19] D. R. Needell *et al.*, "Design criteria for micro-optical tandem luminescent solar concentrators," *IEEE J. Photovolt.*, vol. 8, no. 6, pp. 1560–1567, 2018.

[20] M. A. Green, "Radiative efficiency of state-of-the-art photovoltaic cells," *Prog. Photovolt. Res. Appl.*, vol. 20, pp. 472–476, 2012.

[21] M. A. Green *et al.*, "Solar cell efficiency tables (version 50)," *Prog. Photovolt. Res. Appl.*, vol. 25, no. 7, pp. 668–676, 2017.

[22] Z. Wang *et al.*, "Advanced PERC and PERL production cells with 20.3% record efficiency for standard commercial p-type silicon wafers," *Prog. Photovolt. Res. Appl.*, vol. 20, pp. 260–268, 2012.

[23] M. A. Steiner *et al.*, "Optical enhancement of the open-circuit voltage in high quality GaAs solar cells," *J. Appl. Phys.*, vol. 113, no. 12, pp. 123109–123109-11, 2013.

[24] P. P. C. Verbunt *et al.*, "Increased efficiency of luminescent solar concentrators after application of organic wavelength selective mirrors," *Opt. Express*, vol. 20, no. S5, pp. A655–A668, 2012.

[25] M. G. Debije *et al.*, "Effect on the output of a luminescent solar concentrator on application of organic wavelength-selective mirrors," *Appl. Opt.*, vol. 49, no. 4, pp. 745–751, 2010.

[26] D. N. Chigrin and A. V Lavrinenko, "One-dimensional dielectric periodic structures: Total omnidirectional reflection and spontaneous emission control," *J. Lightw. Technol.*, vol. 17, no. 11, pp. 2018–2024, Nov. 1999.

[27] W. H. Southwell, "Omnidirectional mirror design with quarter-wave dielectric stacks," *Appl. Opt.*, vol. 38, no. 25, pp. 5464–5467, 1999.

[28] H.-Y. Lee and T. Yao, "Design and evaluation of omnidirectional one-dimensional photonic crystals," *J. Appl. Phys.*, vol. 93, no. 2, pp. 819–830, 2003.

[29] A. Arbabi, Y. Horie, M. Bagheri, and A. Faraon, "Dielectric metasurfaces for complete control of phase and polarization with subwavelength spatial resolution and high transmission," *Nat. Nanotechnol.*, no. 10, pp. 937–943, 2014.

[30] Y. Yao, H. Liu, and W. Wu, "Spectrum splitting using multi-layer dielectric meta-surfaces for efficient solar energy harvesting," *Appl. Phys. A*, vol. 115, no. 3, pp. 713–719, 2014.

[31] V. Karagodsky, F. G. Sedgwick, and C. J. Chang-Hasnain, "Theoretical analysis of subwavelength high contrast grating reflectors," *Opt. Express*, vol. 18, no. 16, p. 16973, 2010.

[32] S. Darbe and H. Atwater, "Resonant dielectric high-contrast gratings as spectrum splitting optical elements for ultrahigh efficiency (>50%) photovoltaics," in *Proc. IEEE 42nd Photovolt. Specialist Conf.*, 2015, pp. 1–4.

Authors' photographs and biographies not available at the time of publication.